Methods for measuring 1/1 error field in Wendelstein 7-X stellarator

S.A. Bozhenkov[1], S. Lazerson[2], M. Otte[1], D.A. Gates[2], T.Sunn Pedersen[1] and R.C. Wolf[1]

[1] Max-Planck-Institut für Plasmaphysik, D-17491 Greifswald, Germany
[2] PPPL

E-mail: sergey.bozhenkov@ipp.mpg.de

Abstract. Wendelstein 7-X is an optimized helical axis stellarator that came into operation at the end of 2015. A $m/n = 5/5$ island chain is used in most of its configurations to form a divertor. This island chain at $\iota = 1$ is sensitive to symmetry-breaking error fields, with the resonant 1/1 field being of particular concern because of its influence on the divertor heat flux distribution. Measurement and compensation of the 1/1 mode is therefore necessary. Experimentally, vacuum error fields in W7-X will be studied with a flux surface mapping diagnostic. In this paper numerical simulations for planning and analysing such measurements are presented. Two methods for determining the 1/1 mode are considered: measurement of the island width and measurement of a helical shift of the magnetic axis. Measurement of the resonant island width is a sensitive technique, but the island structure is also affected by other co-resonant components. A complementary method is to measure a helical shift of the magnetic axis in a configuration close to the resonance. This method has a simple interpretation and isolates the 1/1 error field from higher order resonant modes.

1. Introduction

Wendelstein 7-X is an optimized helical axis stellarator with superconducting coils [1]. The non-planar coils were optimized to have a desired geometry of flux surfaces for low neoclassical transport, a high equilibrium β, good MHD properties, a small bootstrap current and a good fast ion confinement. Wendelstein 7-X (W7-X) will be equipped with an island divertor [2,3] and should achieve steady state discharges of up to 30 minutes [4]. The machine operation started at the end of 2015 with a limiter campaign [5].

For the majority of W7-X configurations, a divertor is realized with a 5/5 island chain at the position of the $\iota = 1$ resonance, where ι is rotational transform. Error fields resonant to this rotational transform break the fivefold symmetry, redistribute the divertor heat flux, and might limit the machine performance. The $m/n = 1/1$ error field is the most important here, since it creates a large $m = 1$ island that deposits the heat predominantly on two out of 10 divertor units. A relative 1/1 error field of about $1 \cdot 10^{-4}$ results in an increase of the peak heat flux to one of the divertor modules by a factor of about 2 as predicted by field line tracing with diffusion [6]. Without radiation such an increase can lead to exceeding the design limit of 10 MW/m^2 for the peak heat flux [4]. Simulations of the divertor heat flux with field line tracing are to be considered as an estimation, a more rigorous study is to be performed with EMC3-EIRENE model [7,8]. If radiation losses are excluded, field line diffusion in the symmetric case can be agreed with EMC3-EIRENE by a suitable choice of parameters. Since error fields discussed here strongly change the edge topology, both codes are expected to qualitatively agree. A further discussion of the comparison between field line diffusion and EMC3-EIRENE is beyond the scope of this paper. It is to be noted that in article [6] a numerically different definition of the error field amplitude was used, which resulted in two times larger values.

Error fields appear due to small deviations in shapes and positions of the coils, machine deformations, current leads and ferromagnetic materials. During the W7-X assembly the coil positions were optimized to minimize deleterious field components by taking into account already known errors [9]. In this way, the 1/1 error field due to coil manufacturing and installation was reduced and is predicted to be about $0.15 \cdot 10^{-4}$. A level of about $1 \cdot 10^{-4}$ can be expected for the 1/1 component due to the other sources [9]. Error field amplitude is defined here as amplitude of the normal component of the perturbation field, normalized by the average field on the magnetic axis. A strict definition is given later in the paper.

To compensate the remaining error fields, a set of five trim coils is installed at W7-X [10]. For a successful application of the correction, a method to measure error fields is required. Experimentally, this will be done with a flux surface mapping diagnostic [11, 12]. In this paper numerical simulations supporting measurements of the error fields are presented. The 1/1 field is of the largest concern and must be compensated.

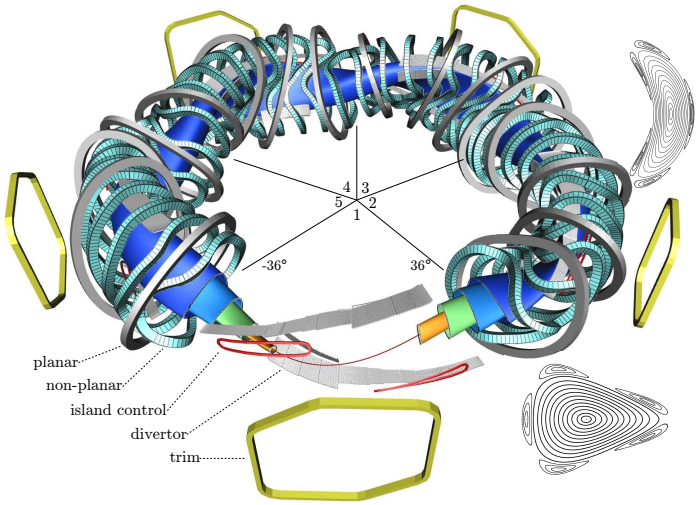

Figure 1. W7-X coil systems and geometry. The non-planar coils are shown in light blue, the planar coils are gray, the island control coils are red, and the trim coils are yellow. The divertor modules are plotted in light gray. The coils in the first module are not shown. Sample flux surfaces and the magnetic axis are plotted in different colors. Poincaré plots in two characteristic planes are presented.

Here two methods for determining the 1/1 mode are considered: measurement of the island width and measurement of a helical shift of the magnetic axis. This paper focuses on the vacuum error fields, plasma effects will be considered separately.

Measurement of the 1/1 error field from the resonant island width is a very sensitive technique, because of a low shear in W7-X. However, the island structure is complicated by the presence of a strong $m/n = 5/5$ intrinsic field and by other possible error fields like 2/2, 3/3. Even if the resonant position is rather close to the magnetic axis, it can be difficult to separate the 1/1 and the 2/2 components. A complementary method of determining the 1/1 amplitude is to measure a helical shift of the magnetic axis in a configuration where the rotational transform is just above 1 at the axis. This method has a simple interpretation and isolates the 1/1 error field from higher order resonant modes.

The article is organized in the following way: in section (2) the W7-X coil systems and the geometry are briefly introduced; in section (3) a mathematical definition of the error field amplitude and its connection to measurable quantities are given; in section (4) the island structure is discussed; in section (5) the off-resonant helical axis shift is analyzed; in section (6) application of the found 1/1 amplitude to other configurations is considered; section (7) summarizes the results.

2. W7-X coils systems and geometry

The geometry and coil systems of Wendelstein 7-X are shown in figure 1. The machine consists of five identical modules, that is there is a fivefold symmetry. Vacuum magnetic flux surfaces are created by the superconducting non-planar and planar coil systems. The non-planar coils, shown in light-blue in figure 1, are optimized modular coils that generate poloidal as well as toroidal component of the main field. There are five types of the non-planar coils, with two coils of the same type per module. The planar coils, shown in dark gray in figure 1, are used to change the horizontal position and to adjust the rotational transform. There are two types of the planar coils, with two coils of each type per module. The non-planar and the planar coils of the same type are connected in series. Besides the main coil systems, there are the island control coils and the error field trim coils. The control coils, two coils per module shown in red in figure 1, are used for fine adjustment of the divertor islands. The trim coils shown in yellow in figure 1 are copper, water-cooled coils to be used mainly for compensation of error fields [10]. Trim coils can also be used to deliberately superimpose magnetic perturbations in order to helically deform the flux surfaces, for example to balance heat flux distribution to the limiters in the case of installation errors [5].

A W7-X magnetic configuration can be described by specifying currents in five types of the non-planar coils and in two types of the planar coils, that is by seven currents. There are several reference configurations planned for experiments. In the standard configuration, all non-planar coils have the same current and the planar coils have zero current. The rotational transform at the edge of the standard configuration is equal to 1 and there is a $m/n = 5/5$ island chain at this position. The rotational transform can be readily changed by the planar coils, figure 2. Planar coil current of the same direction as in the non-planar coils increases the toroidal component of the field thus reducing the rotational transform. Configuration with planar coil current I_{PC} equal to $0.25 \cdot I_{\mathrm{NPC}}$, where I_{NPC} is current in the non-planar coils, is called low-iota and has a $m/n = 6/5$ island chain at the edge. In the case of an opposite current in the planar coils the rotational transform is increased. The case of planar coil current I_{PC} equal to $-0.23 \cdot I_{\mathrm{NPC}}$ is called high-iota configuration. This configuration is suitable for the detection of the 1/1 error field, since the rotational transform at the axis is just above 1. Further reference configurations are discussed in [13, 14].

The geometry of W7-X flux surfaces is three dimensional: the cross-section changes with the toroidal angle. The two most distinct shapes of the cross-section are named triangular and bean shapes. They are illustrated in figure 1. Between these planes there is a gradual transition from one shape to the other.

W7-X will be equipped with an island divertor [2]. The divertor targets intersect an island chain at the plasma edge, thus forming a divertor configuration. There are 10

divertor units installed at the top and the bottom of the machine, figure 1. In an ideal situation the power losses are equally distributed between the targets. Deviations from the fivefold symmetry result in higher heat fluxes to some of the targets. The 1/1 error field is of particular concern and should be reduced to the level of about $0.1 \cdot 10^{-4}$ [6], which corresponds to a tolerable difference in the divertor heat flux of about 10%. To compensate the error fields, five trim coils are available [10]. For a successful compensation a way of measuring the 1/1 error field in the range $(0.1 - 1) \cdot 10^{-4}$ is necessary.

In a stellarator flux surfaces are created solely by external currents; and, consequently, they can be precisely measured without plasma, whereas in tokamaks different plasma response methods are usually used to characterize error fields [15]. Experimental methods for measuring vacuum flux surfaces in stellarator devices are well established. An electron beam is launched along field lines at different locations and intersection points of the beam with a plane can be observed e.g. with a luminescent movable rod [16]. Two such systems are installed in triangular planes in modules 1 and 3 of W7-X, they are toroidally separated by 144°. Both systems have spatial resolution of about 1 cm, as defined by the electron beam size and the imaging optics. In addition, a beam current detection probe is foreseen at the back side of the electron gun for a precise determination of the magnetic axis. Further details of the experimental arrangement are given in [11, 12], details of the camera system can be found in [17].

For numerical studies of the error fields, a W7-X field line tracing web-service is used [6]. This service is available to every user of the W7-X network and can calculate: individual field lines, Poincaré plots, connection lengths, heat fluxes with field line diffusion, magnetic coordinates etc. The tracer uses a realistic first wall represented by an unstructured triangular mesh. With this service it is also possible to calculate an error field spectrum. To simulate individual error field components in this paper, sets of properly aligned filaments with suitable currents are applied.

3. Mathematical definitions

In this section a definition of error field amplitude is given. An error field amplitude is introduced in a magnetic coordinate system. A connection of the given definition to physical measurable quantities like an island width and a flux surfaces shift is discussed.

To give a definition of error field modes, consider field line equations in a curvilinear coordinate system (ρ, θ, φ) [18]:

$$\frac{d\theta}{d\varphi} = \frac{B^\theta}{B^\varphi}$$
$$\frac{d\rho}{d\varphi} = \frac{B^\rho}{B^\varphi}$$

Here $B^i = \vec{B} \cdot \vec{\nabla} x^i$ is a contravariant field component, ρ is a flux surface label and θ, φ

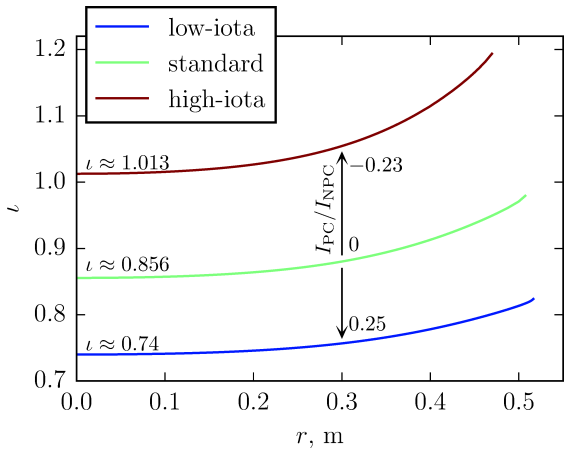

Figure 2. Profiles of rotational transform ι for three reference W7-X configurations: standard, low-iota and high-iota cases. Minor radius r is defined as $\sqrt{\Psi/\pi B_0}$, where Ψ is toroidal flux and B_0 is the field on the axis. Currents in the planar coils I_{PC} relative to the current in the non-planar coils I_{NPC} are given in the plot.

are a poloidal and a toroidal angle correspondingly. The radial field B^ρ is assumed to be a small perturbation, while the poloidal B^θ and the toroidal B^φ components form flux surfaces. If there is no perturbation and a magnetic coordinate system is chosen, that is a coordinate system aligned with field lines, the equation for $d\theta/d\varphi$ gives:

$$\theta = \iota \cdot \varphi + \theta_0, \tag{1}$$

where ι is the angle of the rotational transform normalized by 2π. The equation for $d\rho/\varphi$ defines a flux surface $\rho = const$. In the case of a radial perturbation it is instructive to analyze the radial equation in terms of Fourier harmonics $m\theta + n\varphi$. The mode amplitudes of the right hand side are:

$$b_{mn} \equiv \left(\frac{B^\rho}{B^\varphi}\right)_{mn} = \left(\frac{\vec{B}\cdot\vec{\nabla}\rho}{\vec{B}_0\cdot\vec{\nabla}\varphi}\right)_{mn}, \tag{2}$$

where $\vec{B}_0$ is the unperturbed field. This equation is used as a definition of error field amplitudes, since physically measurable effects are determined by these values.

The expression for error field modes b_{mn} can be reformulated by noting that in a magnetic coordinate system the field is given as [19]:

$$\vec{B}_0 = \frac{d\psi}{d\rho}\cdot\vec{\nabla}\rho\times\vec{\nabla}\theta + \iota\frac{d\psi}{d\rho}\cdot\vec{\nabla}\varphi\times\vec{\nabla}\rho, \tag{3}$$

where ψ is toroidal flux normalized by 2π. With this one finds:

$$b_{mn} = \left(\vec{B}\cdot\vec{\nabla}\psi J\right)_{mn}\cdot\left(\frac{d\rho}{d\psi}\right)^2 = \left(\vec{B}\cdot\left[\frac{\partial\vec{r}}{\partial\theta}\times\frac{\partial\vec{r}}{\partial\varphi}\right]\right)_{mn}\cdot\frac{d\rho}{d\psi} \tag{4}$$

The first expression contains the Jacobian of the coordinate system transformation $J^{-1} = \vec{\nabla}\varphi\cdot(\vec{\nabla}\rho\times\vec{\nabla}\theta)$ and is the same as used for error fields and perturbation

fields in tokamaks [20, 21]. From a practical point of view, the second expression is more useful, because a magnetic coordinate system is usually known as Fourier series of (R, z, φ_g) [6]. The last expression was obtained by representing $\vec{\nabla}\rho$ in terms of covariant vectors $\vec{\nabla}\rho = J^{-1}\,[\partial\vec{r}/\partial\theta \times \partial\vec{r}/\partial\varphi]$.

Units of the mode amplitude b_{mn} in equation 4 depend on the choice of the radial coordinate via the derivative $d\rho/d\psi$. The derivative is often left out, which corresponds to choosing the toroidal flux as a flux label. In such a case the mode amplitudes have units of flux. It is, however, desirable to use a dimensionless quantity that does not depend on the field magnitude and the flux surface radius. In this work the following normalization is assumed:

$$\beta_{mn} = \frac{1}{rR_0B_0} \cdot \left(\vec{B} \cdot \left[\frac{\partial\vec{r}}{\partial\theta} \times \frac{\partial\vec{r}}{\partial\varphi} \right] \right)_{mn}, \tag{5}$$

where R_0 is an average major radius of the axis, B_0 is an average field on the axis and r is a minor radius related to toroidal flux by $\Psi = B_0\pi r^2$. This is the same as choosing the radial coordinate to be minor radius r with an additional normalization by major radius.

If a radial error field is superimposed onto an ideal configuration, the flux surfaces are deformed. A scale of the deformation can be estimated from the field line equations, if the perturbation is small enough to use the unperturbed magnetic angles from equation 1 and to neglect a radial dependence of the perturbation amplitude:

$$|\delta\rho| = \frac{|b_{mn}|}{m\iota + n} \tag{6}$$

In the case of the radial coordinate set to the minor radius r this is:

$$|\delta r| = \frac{R_0|\beta_{mn}|}{m\iota + n} \approx \frac{R_0}{m\iota + n} \cdot \frac{\left(\vec{B} \cdot \vec{n}\right)_{mn}}{B_0} \tag{7}$$

Here $\vec{n}$ is a surface normal and in the last approximation the minor radius is assumed small compared to the major radius. The same result can be obtained by considering equation of a flux surface $\vec{B} \cdot \vec{\nabla}\rho = 0$ [22]. If the rotational transform is close to a resonance the effect of a mode is amplified. For example, for the high-iota configuration the difference between the rotational transform at the axis and 1 is about 10^{-2}; therefore, the mode effect is amplified by a factor of $100 \cdot R_0$.

The shape of the flux deformation in equation 6 depends on the poloidal mode number m. For example, for $m = 0$ the flux surfaces are expanded and compressed radially, for $m = 1$ the flux surfaces are shifted, for $m = 2$ the flux surfaces are elliptically deformed. For the present work the case of $m = 1$ is of interest for measuring the 1/1 error field: the shift of the flux surfaces is proportional to the error field amplitude. Equation 6 is also applicable at the axis [18].

In the case of a resonant error field $m\iota + n = 0$ the solution given by equation 6 is not valid. The deviation of a field line in such a case is limited by the shear. As a field

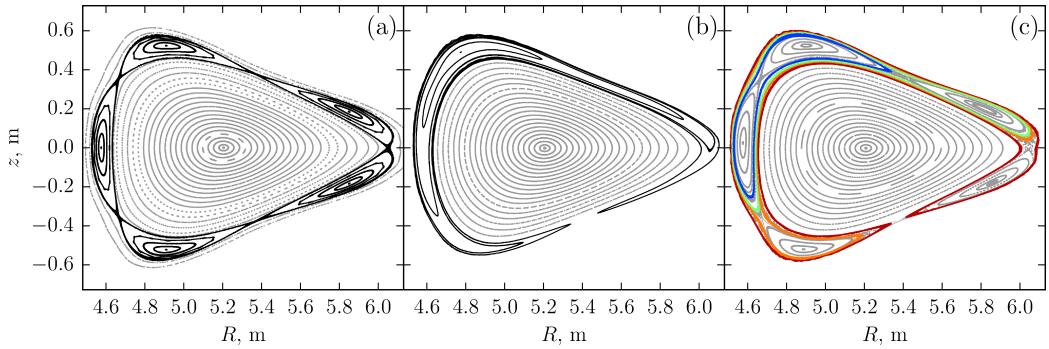

Figure 3. Geometry of edge islands in the standard W7-X configuration. Poincaré plots are shown in the triangular plane. (a) - ideal situation, only the 5/5 independent divertor islands are present; (b) - only the 1/1 error field of $1 \cdot 10^{-4}$, the 5/5 islands are compensated; (c) - superposition of the intrinsic 5/5 islands and the 1/1 error field of $1 \cdot 10^{-4}$. Colors show a structure due to the 1/1 error field.

line departs from the original surface, it runs out of the perturbation phase. A suitable treatment predicts an island of the following full width [23]:

$$w_{mn} = 4 \cdot \sqrt{\frac{b_{mn}}{m d\iota/d\rho}} \tag{8}$$

To measure an island width is the standard way to assess an error field amplitude from flux surface mapping [16]

It is possible to define different magnetic coordinate systems [19]. There are at least three systems in common use: PEST, Hamada, Boozer. Error field amplitudes b_{mn} are different in these systems and need to coincide only in the case of a resonance, for in that case they define the island width [22]. The shift of a surface $\delta\rho$, equation 6, is also measurable and should be the same independent of the used system. This is assured by summing the shifts from different modes, as the spectra are also different. From a practical point of view a choice of the system is not critical, as long as it is used consistently. For the present analysis the Boozer system is chosen.

4. Island structure

Error fields breaking the W7-X fivefold symmetry disturb the intrinsic $m/n = 5/5$ divertor islands. The 1/1 mode has the strongest effect and should be minimized for a successful divertor operation. This requires an ability to measure both its phase and its amplitude. Were there no other co-resonant modes this would be possible by measuring the island width. In practice, additional higher harmonics resonances are present at the same position.

If no error fields are present an intrinsic $m/n = 5/5$ island chain exists at the edge of the standard W7-X configuration, as shown in figure 3a. This Poincaré plot is given in the W7-X triangular plane, which is close to the measurement plane of the flux surface mapping diagnostic [12]. The phase and the amplitude of the intrinsic islands were optimized during the W7-X design for this divertor configuration. The dimensionless amplitude of the intrinsic radial field β_{55} is about $3.2 \cdot 10^{-4}$. It can be expected that for the 1/1 error field to be directly observable with the flux surface mapping diagnostic, its amplitude should be on the order of one fifth of the 5/5 amplitude, that is about $0.6 \cdot 10^{-4}$, where the one fifth is due to the scaling of the island width with the poloidal mode number in equation 8.

An idealized case with only the 1/1 mode of relative amplitude of about $1 \cdot 10^{-4}$ is given in figure 3b. Such an error field would increase the peak heat flux to one of the divertor modules by a factor of two [6]. For this example the intrinsic 5/5 field was compensated with a specially aligned set of filaments producing this component in the counter-phase. In a similar way, the error field was created with an artificial set of filaments. The 1/1 island size is much larger than the resolution of the field line mapping diagnostic. Consequently, such an island could be easily measured.

In practice, the intrinsic 5/5 field cannot be canceled. As a consequence, a combination of the 5/5 and the 1/1 structures appears, figure 3c. Here the error field amplitude is the same as before, but the intrinsic island chain is not compensated. The $m/n = 5/5$ island chain is clearly visible, with an additional 1/1 structure around it. The latter structure is shown in different colors as surfaces surrounding a different number of the internal islands. The outermost surface, dark red in the figure, corresponds to the 1/1 separatrix, which fully encloses all the islands. Smaller surfaces enclose four, three, or two internal islands; they are shown in orange, green and blue correspondingly in the figure. This is in contrast to the situation without the 1/1 error field, where each of the 5 islands is independent and there is a single separatrix between the island chain and the closed flux surfaces. It is by studying this difference that the 1/1 mode can be measured.

Measurement of the 1/1 error field from islands shown in figure 3c can be done in the following way. The area around the 5/5 islands should be thoroughly investigated by changing the electron beam emitter position both poloidally and radially, and the areas with 1/1 structures should be identified. The width of the 1/1 areas is related to the field amplitude, their poloidal position is related to the field phase. Even for a large error field, the geometrical width of the region that differentiates the 1/1 mode can be small. For example for the case shown in figure 3c, in most positions this region is about 1 cm wide and is about 3 cm for the position located at the left top X-point defined by the phase of the used perturbation. Given geometrical limitations of the flux surface mapping diagnostic, e.g. beam size, shadowing by the electron gun and as a consequence a limited number of observable turns, a large uncertainty can be ex-

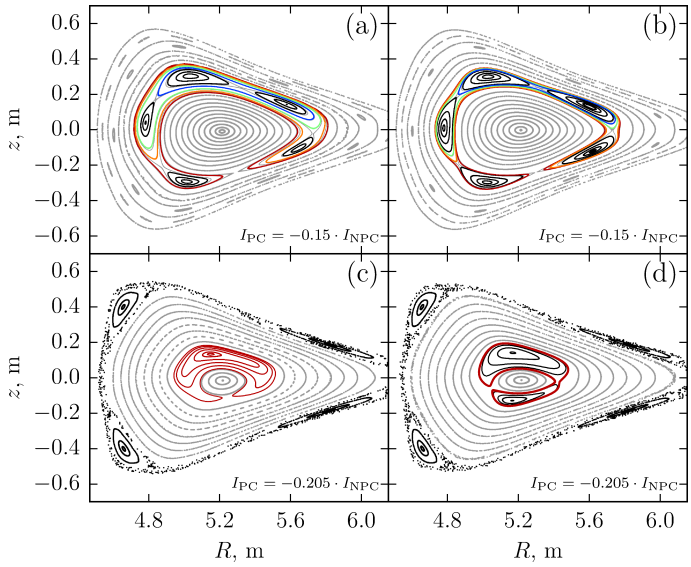

Figure 4. Radial variation of the resonant position $\iota = 1$. Islands in the W7-X triangular plane. (a) - resonant position at $r/a \approx 0.65$, 1/1 error field of amplitude $1 \cdot 10^{-4}$ at the edge. (b) - resonant position at $r/a \approx 0.65$, 1/1 error field of amplitude $0.25 \cdot 10^{-4}$ at the edge. (c) - resonant position at $r/a \approx 0.32$, 1/1 error field of amplitude $0.25 \cdot 10^{-4}$ at the edge. (d) - the same as (c) but with an additional 2/2 field of amplitude $1 \cdot 10^{-4}$ at the edge.

pected [24]. For smaller error field amplitudes, which nevertheless affect the divertor performance, such a measurement is hardly possible. Besides, knowledge of the 5/5 amplitude is required to interpret the results. Additional resonant modes like 2/2, 3/3 etc. can make the interpretation of the measurements cumbersome.

It is possible to separate different error field modes by a radial scan of the resonant position. As the $\iota = 1$ position is shifted towards the magnetic axis, the amplitude of higher poloidal harmonics decays at least linearly, while the 1/1 amplitude stays roughly the same. A further discussion of radial dependence of error fields can be found in section 6. The rotational transform can be varied in a wide range with the aid of the planar coils.

In figure 4a the resonant position is shifted to normalized radius of about 0.65, the 1/1 error field is $1 \cdot 10^{-4}$. Qualitatively the field topology remains the same as in figure 3c, but the region with the 1/1 induced structure shown in colors is much wider. The intrinsic 5/5 field decays radially, whereas the 1/1 error field amplitude does not change. As a result, the measurements can be simplified in this position. For smaller 1/1 amplitudes, such a change of the resonant position is not sufficient. In figure 4b the same resonant position as in figure 4a is used, but the error field amplitude is about $0.25 \cdot 10^{-4}$. For smaller perturbations the error field is visible only in a narrow region. Therefore, to reliably determine the 1/1 error field amplitude in the whole range

of interest, the resonant position should be shifted rather close to the magnetic axis. For further discussion of the resonant position the 1/1 perturbation of $0.25 \cdot 10^{-4}$ is used.

In figure 4c the $\iota = 1$ position is shifted to normalized radius of about 0.32. The 1/1 error field amplitude is the same as in the previous example. For this position the intrinsic islands are not visible anymore. The 1/1 island has a clear structure and a large width because of a very low shear in the center. The island width measurement close to the axis is very sensitive even to small error fields. Since the width scales with the square root of the perturbation amplitude, an island sufficiently large for the surface mapping diagnostic is excited in the whole range of interest of the 1/1 amplitude. A further shift towards the axis leads to an overlapping of the island and the axis, that is a clear island structure could not be observed. The resonant position in figure 4c is about the deepest for a clean island measurement. Obviously, the deepest position changes with the perturbation amplitude.

If a 2/2 error field of a sufficiently large amplitude is present in addition to the 1/1 field, the island structure changes. In figure 4d the same resonance position and the same 1/1 field are used as in the previous figure. But in addition, the 2/2 mode of amplitude of about $1 \cdot 10^{-4}$ at the edge is applied. Both error field components are roughly the same at the resonant position. The 2/2 islands are predominantly seen, the 1/1 structure is highlighted with dark red and is hard to recognize. From this one can conclude that in the case of a strong 2/2 error field a weak 1/1 mode cannot be measured directly. This is partially because the resonant position should stay off the axis for a clean island observation.

A reliable measurement of the 1/1 error field requires a considerable shift of the resonant position to the magnetic axis. The deepest position is limited by a sufficient distance to the axis for an island to be visible. If higher harmonics of a sufficient amplitude are present in addition to the 1/1 field, it can be hard to measure the latter directly. A measurement is still possible by first compensating the higher mode with the trim coils, which is also required for the divertor operation. Alternatively, a helical shift of the magnetic axis in a slightly off-resonance configuration can be used to better isolate the 1/1 component, as detailed in the next section.

5. Helical shift of flux surfaces

In W7-X the rotational transform can be raised with the help of the planar coils so, that the $\iota = 1$ resonance is not present, but the value at the axis is very close to that. For example, the high-iota configuration, figure 2, has these properties. In this case, the flux surfaces are distorted by an error field and the amplitude of the distortion can be related to the error field from equation 7. In particular, an 1/1 field results in a shift of

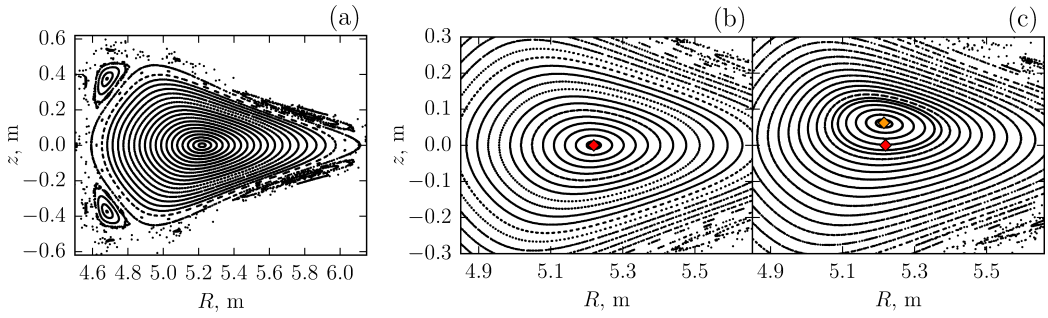

Figure 5. Magnetic axis shift by the 1/1 error field in high-iota configuration. (a) - overview of the high-iota configuration, $m/n = 4/5$ islands and partially stochastic field lines at the edge; (b) - central flux surfaces and the magnetic axis; (c) - central flux surfaces and the axis with the 1/1 error field of $2 \cdot 10^{-4}$. The error field phase is chosen to result in an upward shift.

the flux surfaces. For an error field of $1 \cdot 10^{-4}$ and for high-iota configuration, the shift is estimated to be about 5 cm. Such a value is accessible experimentally with the W7-X flux surface mapping diagnostic. Therefore, this effect can also be used to measure the 1/1 error field. Advantages of this method are that the flux surfaces have a simple geometry, and that the higher order harmonics have the smallest possible amplitude.

Displacement of flux surfaces due to a perturbation close to the resonance can be used to access the 1/1 error field. In high-iota configuration the rotational transform at the magnetic axis is very close to one, with the difference being about 0.013. A corresponding Poincaré map is given in figure 5a. There are $m/n = 4/5$ islands at the edge with probably some ergodic field lines around. If an 1/1 error field is added, flux surfaces in the center, where ι is very close to 1, are significantly shifted. In figure 5b ideal flux surfaces in the center are shown and in figure 5c flux surfaces with the 1/1 perturbation of $2 \cdot 10^{-4}$ are given. For the chosen perturbation phase, the surfaces are shifted upwards. The shift decreases as the minor radius increases, because the distance to the resonance becomes larger. It is convenient to quantify this effect by the axis shift. Positions of the axes are marked in the figures. For this example the axis is shifted by about 6 cm. The absolute value of the shift changes with the phase because of the elliptical shape of the flux surfaces.

The magnitude and the direction of the axis shift depend on the amplitude and the phase of the 1/1 field. In figure 6, positions of the magnetic axis in the triangular plane are shown for five different perturbation amplitudes and for a full range of phases. The larger the error field amplitude is, the larger is the shift. Axis positions complete a full turn around the unperturbed axis, as the error field phase is changed from 0 to 2π. Major phase directions are presented in the figure with dashed lines. For a given perturbation amplitude, the absolute value of the axis shift changes with the phase: for the triangular plane the contours are elongated in the horizontal direction

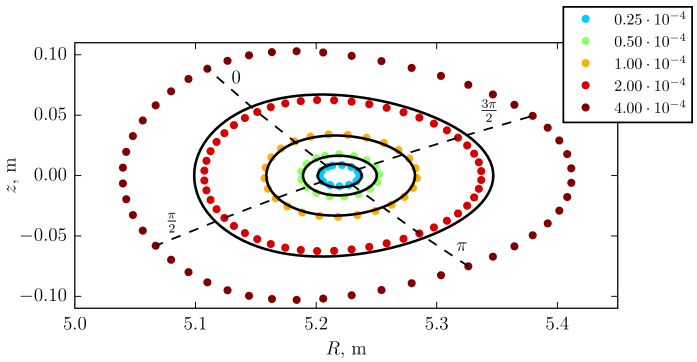

Figure 6. Magnetic axis position for the 1/1 error field of different amplitudes and phases in the high-iota configuration. The error field phase is scanned from 0 to 2π for each amplitude. Solid black lines show position expected according to equation 7 for ι at the axis. Dashed black lines show phase directions 0, $\pi/2$, π and $3\pi/2$.

by a factor of about 1.8. For example, for the case $2 \cdot 10^{-4}$ the horizontal change is about 11 cm, whereas the vertical one is about 6 cm. For an 1/1 error field weaker than $0.2 \cdot 10^{-4}$, the smallest shift in this configuration is below the resolution of the W7-X flux surface mapping diagnostic. In other cases, both the phase and the amplitude of the error field can be determined from the axis position. It follows from equation 7 that a phase scan for a fixed amplitude is an unperturbed flux surface of radius coinciding with the deviation $r = \delta r_{11}$. Here radial coordinate r is to be considered as an effective "average" radius. In figure 6 such flux surfaces are given with black lines for all but one case. For the largest 1/1 amplitude the surface is not plotted, for the discrepancy with the numerical result becomes large. For amplitudes below about $2 \cdot 10^{-4}$, i.e. for shifts δr less than about 9 cm, the deviation can be related to the perturbation amplitude via equation 6 with accuracy of better than 10%, if the geometrical expansion factor is included. For larger deviations the shear has to be taken into account, which can be done numerically.

The amplitude of the axis shift can be considerably increased, if the rotational transform is further adjusted towards the resonance. A dependence of the axis shift on the rotational transform is illustrated in figure 7 for three values of the 1/1 amplitude. The shown calculations are for the error field phase resulting in a vertical shift of the axis, which is about two times smaller than the corresponding horizontal shift in the triangular plane. In the considered range of ι the deviation is changed by a factor of about 5. Deviations estimated from equation 7 for the three cases are given with dashed lines in the figure. The calculated values differ from the numerical ones above approximately 5 cm, because of a noticeable shear. Since the shift depends linearly on the perturbation, the adjustment of the rotational transform is required to cover the required range of the 1/1 amplitudes $(0.1 - 1) \cdot 10^{-4}$.

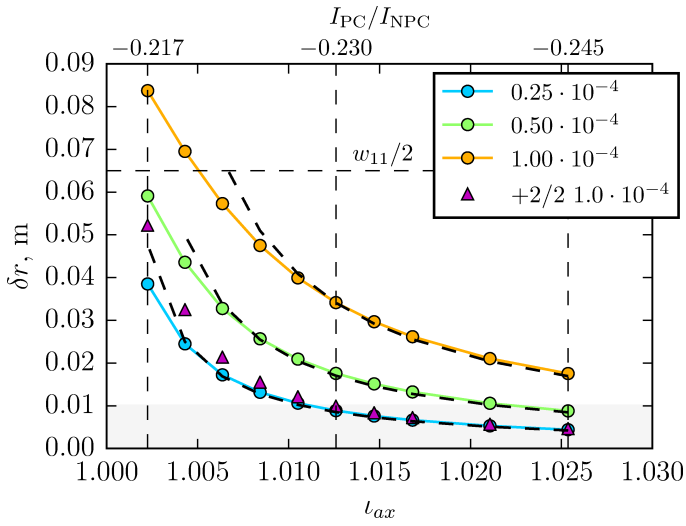

Figure 7. Axis shift due to the 1/1 error field for different values of the rotational transform at the axis. Three values of the planar coils current I_{PC} relative to the current in the non-planar coils I_{NPC} are given in the plot. Axis positions are given for three amplitudes of the 1/1 field and for a superposition of the 1/1 field of $0.25 \cdot 10^{-4}$ and of the 2/2 field of $1 \cdot 10^{-4}$. For a comparison, resolution of the W7-X flux surface diagnostic is about 1 cm [12].

For configurations with a negative current in the planar coils, decreasing the rotational transform corresponds to decreasing the absolute value of the current in the planar coils. Three values of the planar coil currents, two boundary values and the value for the high-iota configuration, are given in the plot as well. A change of 0.01 in the relative planar coil current means a change of about 400 A per winding for a configuration with field of 2.5 T at the axis. That is, such a study is accessible experimentally. The lowest achievable difference to the resonance will be given by the accuracy of the current control and by applicability of the flux surface mapping diagnostic due to shadowing by the emitter head.

Helical axis shift in an off-resonance configuration is smaller than the width of the equivalent 1/1 island. The half-width of the 1/1 island excited by the error field of about $0.25 \cdot 10^{-4}$ is plotted as a horizontal line in figure 7. Such an island is shown in figure 4c. The amplitude of the axis shift can be raised to about one third of the island width by adjusting the rotational transform in the considered range. On the other hand, the observed axis shift is weakly sensitive to additional error field components. For example, even in the case of a 4 times stronger 2/2 field at the edge, the axis shift can still be used to measure the 1/1 amplitude within about 20%, as shown in figure 7 with triangles. In addition, the 2/2 error field deforms the flux surfaces, which could be distinguished. The error field superposition used for this example is the same as in figure 4d.

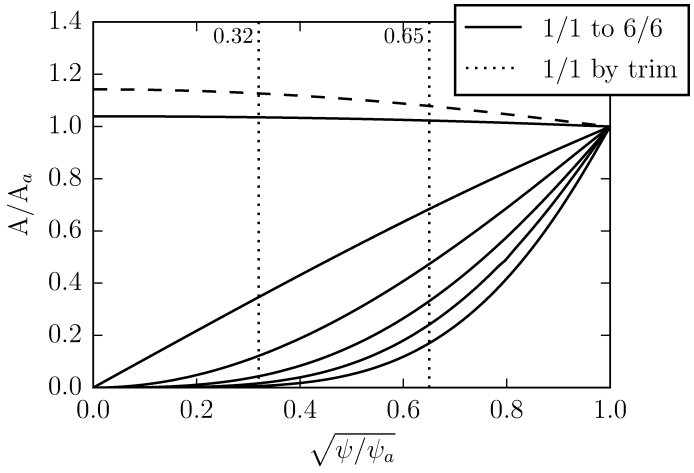

Figure 8. Radial scaling of error fields for the standard W7-X configuration. Solid lines show amplitudes of separate modes from 1/1 to 6/6. Dashed line shows the 1/1 amplitude excited by the trim coils with a $n = 1$ current distribution. Vertical lines mark the radial positions used in figure 4.

The axis position can be measured either directly with a current sensor detecting the electron beam or from camera images of sufficiently small flux surfaces. To measure the 1/1 amplitude, the ideal axis position is also required. The ideal axis can be measured from flux surfaces of sufficiently large radius in the same configuration or in a configuration further away from the resonance. In both cases the remaining influence of the 1/1 error field can be reduced to about 10% of the axis distortion close to resonance, because the achievable difference $\iota - 1$ is of the order of 0.1. The ideal axis position changes weakly with rotational transform, e.g. for the mentioned case of $\iota_{\mathrm{ax}} - 1 \approx 0.1$ at the axis the ideal axis change is about 5 mm. The accuracy of finding the ideal axis from large radius flux surfaces is given by experimental restrictions. The rotational transform ι can be determined with a flux surface mapping diagnostic as well [16]. Further details concerning experimental measurements are given in [12, 24].

6. Application of results

Methods described in this paper provide measurements of 1/1 error field amplitude in a dedicated magnetic configuration with the resonance position close to the magnetic axis. From a practical point of view, the 1/1 error field should be compensated in a variety of configurations with resonant position mainly at the edge. In this section, scaling of the 1/1 amplitude with the radius and to the other W7-X reference configurations having slightly different flux surface shapes is briefly discussed. Moreover, the radial scaling of error fields presented here explains the need for a deep resonant position.

Error fields discussed in this paper are vacuum fields. Such fields are described by the Laplace equation for scalar potential with corresponding boundary conditions on a

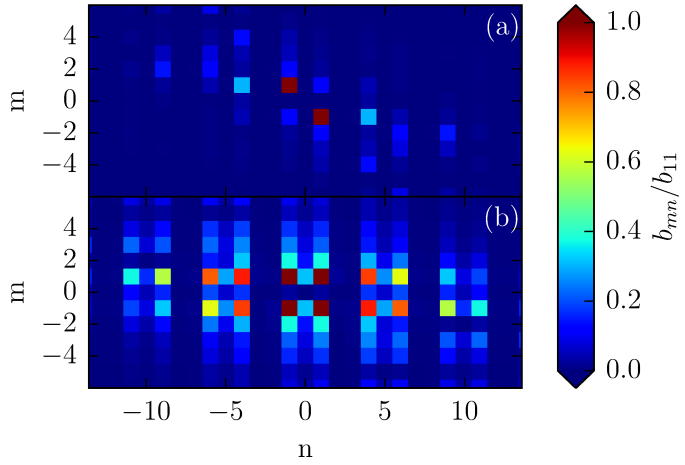

Figure 9. A comparison of the error spectrum produced (a) by dedicated filaments for the 1/1 error field, and (b) by the trim coils with the $n = 1$ current distribution. Shown are complex Fourier series $e^{i(m\theta+n\varphi)}$ normalized to the 1/1 amplitude.

reference surface.In a periodic cylinder, modes with poloidal m and toroidal n numbers are independent and their amplitudes are given by modified Bessel functions of the first kind $I_m(nr/R)$ [25]. As a consequence, the radial field component is proportional to r^{m-1} for a sufficiently small radius. That is the poloidal mode $m = 1$ remains constant, while other modes decay at least linearly. It is this behaviour that is used to isolate the 1/1 error field in this paper.

Magnetic coordinates used to define error field amplitudes in W7-X are more complicated than a periodic cylinder. Already in a torus the m/n mode amplitude is not independent: in the equation for the mode m there are coupling terms to the modes $m \pm 1$, which are of the order of the inverse aspect ratio. For W7-X magnetic coordinates, the coupling of the 1/1 error field is analyzed numerically. A mode m/n of unit amplitude at the edge is created with a dedicated set of filaments. The resulting amplitude of the 1/1 field in the center is taken as a measure of the influence of the m/n mode. In such a way it is found that the modes with the strongest coupling are $m \pm 1$, $m \pm 2$ and $n \pm 5$. Additional toroidal modes appear because of the fivefold symmetry.

Figure 8 demonstrates a radial dependence of several error field modes for the standard W7-X configuration in the Boozer coordinates. Solid lines in the figure are for individual modes from 1/1 to 6/6 created with dedicated sets of filaments. As expected, a mode with poloidal number m decays according to r^{m-1}. Observed deviations can be explained by the toroidal coupling discussed above. Vertical lines in the figure show positions used in figure 4 to show a change of the island structure with radius. It follows from figure 8 that the resonant position should be placed closer than about 0.5 for the intrinsic island chain to become insignificant compared with a weak 1/1 error field. In a

similar way, the 2/2 error field attenuation is not sufficient at the position with enough clearance between the islands and the axis.

If the error field spectrum includes further components, the 1/1 field change with radius becomes larger, as illustrated with a dashed line in figure 8. This case shows the 1/1 error field excited by the trim coils with $n = 1$ current distribution. In this case the spectrum has additional components, which results in about 10% change of the 1/1 amplitude from the edge to the center. A comparison of error spectra produced by a set of filaments established for the 1/1 field and by the trim coils is given in figure 9. Amplitudes of Fourier series $e^{i(m\theta+n\varphi)}$ in this figure are normalized to the corresponding 1/1 amplitudes. The trim coils spectrum contains additional modes, since there are only 5 discrete coils. A further discussion of the compensation of the intrinsic 1/1 error field with the trim coils and of radial scaling of the compensated mode is beyond the scope of this paper.

The W7-X configuration space is very wide. A change of the flux surface geometry means a change in the definition of magnetic coordinates and, consequently, in the error field amplitudes. A possible order of magnitude of this change is studied numerically by setting up a dedicated m/n mode in the standard W7-X configuration and measuring the 1/1 amplitude for a configuration of interest. For this paper, the W7-X reference configurations [13] were analyzed. The modes 0/1, 0/4, 1/4 and 2/6 defined for the standard configuration are found to contribute up to a quarter of their amplitudes to the 1/1 amplitude in other configurations. A practical example is a change of the 1/1 amplitude produced by the trim coils. In this case the change from a configuration to configuration is found to be at most 10%.

The numerical analysis in this section supports the isolation of the 1/1 error field from other poloidal modes by placing the resonant position close to the magnetic axis. The 1/1 amplitude can change radially and from a configuration to configuration depending on the other components. Therefore, some care could be required while applying the results for the 1/1 error field compensation.

7. Summary

In most of the Wendelstein 7-X configurations, a divertor is realized with a 5/5 island chain at the position of the $\iota = 1$ resonance. Error fields resonant to this rotational transform break the fivefold symmetry and might limit the machine performance. The 1/1 error field is the most important here, since it creates a large $m = 1$ island and concentrates the heat flux on two out of 10 divertor modules. The 1/1 error field of about $1 \cdot 10^{-4}$ results in an increase of the peak heat flux to one of the divertor modules by a factor of about 2 [6]. In this article methods of measuring the vacuum 1/1 amplitude were analyzed numerically.

Two methods of determining the 1/1 amplitude were considered: measurement of the island width and measurement of a helical shift of the magnetic axis. Measurement of the 1/1 error field from the resonant island width is a well known technique, which is very sensitive in W7-X because of a low shear. A complementary method of determining the 1/1 amplitude is to measure a helical shift of the magnetic axis in a configuration where the rotational transform is just above 1. This method is experimentally simple and isolates the 1/1 error field from higher order resonant modes.

Measurement of the 1/1 error field using W7-X configurations with the resonant $\iota = 1$ position at the edge is found to be challenging because of a large intrinsic 5/5 island chain. The error field can be at least theoretically observed on top of the 5/5 islands, if the perturbation is large enough. Practically, even for the 1/1 field of about $1 \cdot 10^{-4}$ the width of the layer differentiating it from the intrinsic islands is of the order of 1 cm for most poloidal positions and is about 3 cm for the optimal position determined by relative phase of the 1/1 perturbation. The resolution of the W7-X flux surface mapping diagnostic is of the order of 1 cm [12]. The island structure measurements require a careful exploration of the full poloidal cross-section and are likely to have a large uncertainty. Additional resonant modes like 2/2, 3/3 etc. can make a direct measurement of the error fields difficult.

Error field modes can be separated by choosing a magnetic configuration with the resonant position shifted towards the magnetic axis. The amplitude of a poloidal mode m decays as r^{m-1}, as it found for a periodic cylinder. That is the 1/1 field stays constant, whereas the other components decay at least linearly. A resonant position variation can be easily achieved in W7-X by applying the planar coils.

To clearly separate the 1/1 error field from the intrinsic 5/5 field, the normalized radius of the resonant position should be less than about 0.5. If an additional much stronger 2/2 error field is present, the 1/1 island structure is still disturbed even close to the axis. In such a situation, the measurement could be performed by first compensating the dominant error field with the trim coils.

A complementary method for measuring the 1/1 error field is to measure a helical axis shift in a configuration, where there is no resonance but the rotational transform at the axis is close to resonance. For example, the W7-X high-iota configuration turns out to be suitable for this purpose. Advantages of this method are that the flux surfaces have a simple geometry, and that the higher order harmonics have the smallest possible amplitude. The flux surface distortion depends linearly on the perturbation amplitude.

The amplitude and the phase of the helical axis shift is directly related to the amplitude and the phase of the 1/1 error field. The shift for the error field of about

$1 \cdot 10^{-4}$ is found to be of the order of 5 cm in the high-iota configuration. Thus, it can be reliably measured with the flux surface mapping diagnostic. The perturbation phase can be concluded from the shift direction. The sensitivity of the method can be further increased by adjusting the rotational transform on the axis towards the resonance. The shift is inversely proportional to the difference of the rotational transform and one. Such an adjustment is required to measure the 1/1 error field of about $0.1 \cdot 10^{-4}$ with the help of the W7-X flux surface mapping diagnostic. If the rotational transform on the axis is shifted away from 1 the unperturbed axis can be measured. The axis shift is smaller than a corresponding island width, but is rather insensitive to other error field modes, e.g. to the 2/2 field.

The two methods for measuring the 1/1 error field considered here form a basis for experiments with the flux surface mapping diagnostic. They are sufficiently sensitive in the expected range of amplitudes and can be applied depending on the presence of other error field components. A certain care should be taken in applying the found amplitude to other W7-X magnetic configuration. Since the error field amplitudes are defined in the magnetic Boozer coordinates, the numerical value can change from configuration to configuration. The discussion in this paper deals only with vacuum error fields, plasma response to the error fields will be analyzed separately. For the most important case of the error field compensation in divertor configurations, such effects are expected to be small, because the region of interest is located at the plasma edge.

8. Acknowledgment

This work has been carried out within the framework of the EUROfusion Consortium and has received funding from the Euratom research and training programme 2014-2018 under grant agreement No 633053. The views and opinions expressed herein do not necessarily reflect those of the European Commission.

References

[1] Grieger G, Beidler C, Harmeyer E, Junker J, Kißlinger J, Lotz W, Merkel P, Montvai A, Nührenberg J, Rau F, Schlüter A, Wobig H and Zille R 1989 Physics studies for helical-axis advanced stellarators Plasma Physics and Controlled Nuclear Fusion Research, Proceedings of the 12th International Conference, Nice, 1988 vol 2 (IAEA, Vienna) pp 369 – 387

[2] Kißlinger J, Beidler C D, Harmeyer E, Rau F, Renner H and Wobig H 1994 Island divertor for the stellarator Wendelstein 7-X Controlled Fusion and Plasma Physisc, Proceedings of 21st European Conference, Montpellier, 1994 vol 18B, part 1 (European Physical Society, Geneva) pp 368 – 371

[3] Greuner H, Bitter W, Kerl F, Kißlinger J and Renner H 1995 Structure of divertor for the optimized stellarator W7-X Fusion Technology, Proceedings of 18th Symposium Karlsruhe, 1994 vol 1 (Elsevier, Amsterdam and New-York) pp 323 – 326

[4] Renner H, Boscary J, Erckmann V, Greuner H, Grote H, Sapper J, Speth E, Wesner F and Wanner M 2000 Nuclear Fusion **40** 1083 – 1093

[5] Pedersen T S, Andreeva T, Bosch H S, Bozhenkov S, Effenberg F, Endler M, Feng Y, Gates D, Geiger J, Hartmann D, Hlbe H, Jakubowski M, Knig R, Laqua H, Lazerson S, Otte M, Preynas M, Schmitz O, Stange T, Turkin Y and the W7-X Team 2015 Nuclear Fusion **55** 126001 URL http://stacks.iop.org/0029-5515/55/i=12/a=126001

[6] Bozhenkov S, Geiger J, Grahl M, Kißlinger J, Werner A and Wolf R C 2013 Fusion Engineering and Design **88** 29973006

[7] Feng Y, Kobayashi M, Lunt T and Reiter D 2011 Plasma Physics and Controlled Fusion **53** 024009 URL http://stacks.iop.org/0741-3335/53/i=2/a=024009

[8] Feng Y, Frerichs H, Kobayashi M, Bader A, Effenberg F, Harting D, Hoelbe H, Huang J, Kawamura G, Lore J D, Lunt T, Reiter D, Schmitz O and Sharma D 2014 Contributions to Plasma Physics **54** 426–431 ISSN 1521-3986 URL http://dx.doi.org/10.1002/ctpp.201410092

[9] Andreeva T, Bruer T, Bykov V, Egorov K, Endler M, Fellinger J, Kilinger J, Kppen M and Schauer F 2015 Nuclear Fusion **55** 063025 URL http://stacks.iop.org/0029-5515/55/i=6/a=063025

[10] Rummel T, Rißе K, Kißlinger J, Koppen M, Fullenbach F, Neilson H, Brown T and Ramakrishnan S 2012 Applied Superconductivity, IEEE Transactions on **22** 4201704 ISSN 1051-8223

[11] Bosch H S, Brakel R, Gasparotto M, Grote H, Hartmann D, Herrmann R, Nagel M, Naujoks D, Otte M, Risse K, Rummel T and Werner A 2014 Plasma Science, IEEE Transactions on **42** 432–438 ISSN 0093-3813

[12] Otte M, Amus D, Biedermann C, Bozhenkov S, Braeuer T, Dudek A, Geiger J, Kocsis G, Lazerson S, Sunn Pedersen T, Schauer F, Szepesi T and Standley B 2016 submitted to PPCF

[13] Andreeva T, Kisslinger J and Wobig H 2002 Characteristics of main configurations of wendelstein 7-x Problems of Atomic Science and Technology Series: Plasma Physics vol 4 (Kharkov: National Science Center, Kharkov Institute of Physics and Technology) pp 45–47 URL http://vant.kipt.kharkov.ua/ARTICLE/VANT_2002_4/article_2002_4_45.pdf

[14] Geiger J, Beidler C D, Feng Y, Maaberg H, Marushchenko N B and Turkin Y 2015 Plasma Physics and Controlled Fusion **57** 014004 URL http://stacks.iop.org/0741-3335/57/i=1/a=014004

[15] Strait E, Buttery R, Casper T, Chu M, Hanson J, Garofalo A, Gribov Y, Haye R L, Reimerdes H, Schaffer M and Volpe F 2014 Nuclear Fusion **54** 073004 URL http://stacks.iop.org/0029-5515/54/i=7/a=073004

[16] Jaenicke R, Ascasibar E, Grigull P, Lakicevic I, Weller A, Zippe M, Hailer H and Schworer K 1993 Nuclear Fusion **33** 687 URL http://stacks.iop.org/0029-5515/33/i=5/a=I02

[17] Kocsis G, Baross T, Biedermann C, Bodnr G, Cseh G, Ilkei T, Knig R, Otte M, Szabolics T, Szepesi T and Zoletnik S 2015 Fusion Engineering and Design **9697** 808 – 811 ISSN 0920-3796 proceedings of the 28th Symposium On Fusion Technology (SOFT-28) URL http://www.sciencedirect.com/science/article/pii/S0920379615001581

[18] Solov'ev L and Shafranov V 1970 Plasma confinement in closed magnetic systems (Reviews of Plasma Physics vol 5) (Consultants Bureau)

[19] D'haeseleer W, Hitchon W N G, Callen J D and Shohet J 1991 Flux Coordinates and Magnetic Field Structure (Springer-Verlag Berlin)

[20] Paz-Soldan C, Buttery R, Garofalo A, Hanson J, Haye R L, Lanctot M, Park J, Solomon W and Strait E 2014 Nuclear Fusion **54** 073013 URL http://stacks.iop.org/0029-5515/54/i=7/a=073013

[21] Schaffer M, Menard J, Aldan M, Bialek J, Evans T and Moyer R 2008 Nuclear Fusion **48** 024004 URL http://stacks.iop.org/0029-5515/48/i=2/a=024004

[22] Park J k, Boozer A H and Menard J E 2008 Physics of Plasmas **15** 064501 URL http://scitation.aip.org/content/aip/journal/pop/15/6/10.1063/1.2932110

[23] Boozer A H 2005 Rev. Mod. Phys. **76**(4) 1071–1141 URL http://link.aps.org/doi/10.1103/RevModPhys.76.1071

[24] Lazerson S, Otte M, Bozhenkov S, Sunn-Pedersen T, Bruer T, Gates D and Neilson G H 2015 Modeling and analysis of flux surface mapping experiments on W7-X 57th Annual Meeting of the APS Division of Plasma Physics (APS 2015)

[25] Jackson J D 1999 Classical Electrodynamics third edition ed (John Wiley & Sons, Inc.)